Chinese Journal of Catalysis 36 (2015) 1142–1154

available at www.sciencedirect.com

ScienceDirect

journal homepage: www.elsevier.com/locate/chnjc

Article

Oxidative carbonylation of phenol with a Pd-O/CeO_2-nanotube catalyst

Ye Yuan, Zhimiao Wang, Hualiang An, Wei Xue *, Yanji Wang #

Hebei Provincial Key Laboratory of Green Chemistry & High Efficient Energy Saving, School of Chemical Engineering and Technology, Hebei University of Technology, Tianjin 300130, China

ARTICLE INFO

Article history:
Received 22 December 2014
Accepted 7 February 2015
Published 20 July 2015

Keywords:
Diphenyl carbonate
Oxidative carbonylation
Ceria nanotube
Palladium catalyst
Temperature-programmed reduction
Surface oxygen

ABSTRACT

CeO_2 nanotubes (CeO_2-NT) were synthesized using carbon nanotubes as template by a liquid phase deposition and hydrothermal method. X-ray diffraction, transmission electron microscopy, and N_2 adsorption-desorption were used to characterize the CeO_2-NT. The wall of CeO_2-NT was composed of small interconnected nanocrystallites ranging from 4 to 9 nm in size. The specific surface area of CeO_2-NT was 108.8 m^2/g with an outer diameter of 25 nm and length > 300 nm. Supported Pd catalyst, Pd-O/CeO_2-NT, was prepared using CeO_2-NT as the support. Temperature-programmed reduction analysis showed that the surface oxygen on Pd-O/CeO_2-NT could be reduced at low temperature, therefore it showed high activity in the reaction. Pd-O/CeO_2-NT was used as the catalyst for the oxidative carbonylation of phenol. It has better activity and DPC selectivity than Pd-O/CeO_2-P, which was prepared by supporting Pd on zero dimensional CeO_2 particles. Under the optimized conditions, phenol conversion was 67.7% with 93.3% DPC selectivity with Pd-O/CeO_2-NT. However, its catalytic activity decreased when the catalyst was used for the second time. This was attributed to the destruction of the tubular structure of Pd-O/CeO_2-NT and Pd leaching during the reaction.

1. Introduction

Diphenyl carbonate (DPC) is an important chemical intermediate for many organic compounds and polymers such as polycarbonates, *p*-hydroxybenzoic acid polyesters, and aliphatic monoisocyanates [1,2]. In recent years, the synthesis of DPC has received more attention due to the extensive use of polycarbonates [3]. The industrial synthesis of DPC is based on the highly toxic phosgene [1]. There are also two non-phosgene methods, transesterification [4,5] and oxidative carbonylation of phenol [6], which are under study. Among these, the oxidative carbonylation of phenol with CO and O_2, shown in Eq. (1), is an attractive method as it is a one-step process with H_2O being the sole byproduct in principle.

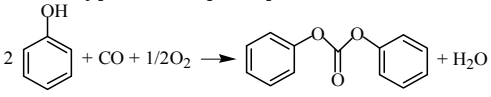

(1)

The oxidative carbonylation of phenol is a multi-step electron transfer reaction [7]. It is normally catalyzed by Pd compounds with various co-catalysts [8–20]. Vavasori et al. [7] studied the reaction using $Pd(OAc)_2$ or $PdBr_2$ as catalyst, along with benzoquinone and Co, Mn, and Cu salts as cocatalysts. In particular, the influence of the cocatalysts was discussed. Xue et al. [10] prepared an embedded Pd-Cu-O/SiO_2 catalyst using a

* Corresponding author. Tel: +86-22-60202419; Fax: +86-22-60204697; E-mail: weixue@hebut.edu.cn
# Corresponding author. Tel: +86-22-60202419; Fax: +86-22-60204697; E-mail: yjwang@hebut.edu.cn
This work was supported by the National Natural Science Foundation of China (21236001, 21176056, 21106031), the Programme for 100 Excellent Talents in University of Hebei Province (II) (BR2-208), and the Natural Science Foundation of Hebei Province (B2015202228).
DOI: 10.1016/S1872-2067(14)60312-0 | http://www.sciencedirect.com/science/journal/18722067 | Chin. J. Catal., Vol. 36, No. 7, July 2015

water-in-oil microemulsion as nano-reactors. Its catalytic performance with $Cu(OAc)_2$, hydroquinone, and tetrabutylammonium bromide (TBAB) acting as cocatalysts was evaluated. The DPC yield was 35.4% with reduced Pd leaching and improved stability. Ce compounds are effective cocatalysts for the homogenerous Pd-catalyzed oxidative carbonylation of phenol [8]. In addition, Ce can also be used as the second metal component or support, in the form of CeO_2, as the heterougeneous catalyst for this reaction. Wu et al. [21] prepared a Pd catalyst supported on Mn-doped CeO_2 for the oxidative carbonylation of phenol and obtained a DPC yield of 9.3%. Wang [22] reported a Pd-Ce-O/SiO_2 catalyst prepared by microemulsion that gave 53.7% DPC yield under optimized conditions.

CeO_2 with the fluorite structure is a significant rare earth oxide in industrial catalysis. It can act as an oxygen buffer by absorbing and releasing oxygen through a fast Ce^{3+}/Ce^{4+} cycle involving the participation of the lattice oxygen species. It has been extensively studied and applied in heterogeneous catalysis [23–27]. Usually, its unique redox property is dependent on the size of the CeO_2 particles. The morphology also influences the redox feature of CeO_2 significantly through the exposed crystalline planes. A typical example is CeO_2 nanorods with a one-dimensional structure, which showed a higher CO oxidation activity than other conventional nanoparticles due to the exposed (110) crystal surface of CeO_2 [28,29]. In addition, CeO_2 nanotubes also show excellent activity for CO oxidation. This was explained by the combination of the large surface-to-volume area with the inner side of the nanotubes providing more active sites [28,30]. Therefore, a good catalytic performance for DPC synthesis utilizing CeO_2 with the one-dimensional structure as the support for a heterogeneous Pd catalyst is expected.

In this work, CeO_2 nanotubes (CeO_2-NT) and a Pd-O/CeO_2-NT catalyst were synthesized by the liquid phase deposition-hydrothermal method using carbon nanotubes (CNTs) as the template. The catalytic performance for the oxidative carbonylation of phenol to DPC was evaluated and compared with that using zero-dimensional CeO_2 nanoparticles supporting a Pd catalyst. The effects of the reaction conditions were also studied for the Pd-O/CeO_2-NT catalyst.

2. Experimental

2.1. Preparation of Pd-O/CeO_2-NT catalyst

A 4 g sample of CNTs (length 0.5–2 μm, outer diameter 30–50 nm, purity > 95%, Chengdu Organic Chemistry Co., Ltd., Chinese Academy of Sciences) was heated in 30% HNO_3 (600 mL) under reflux at 120 °C for 24 h. Then the CNTs were cooled to room temperature. After that, they were separated by filtration and washed with deionized water and anhydrous ethanol repeatedly until pH = 7. The CNTs were dried at 80 °C.

CeO_2-NT was synthesized by the liquid phase deposition [31] hydrothermal method using the pretreated CNTs as the template. First, the CNTs (0.54 g) were dispersed in a solution composed of $Ce(NO_3)_3$ aqueous solution (0.15 mol/L, 20 mL) and anhydrous ethanol (215 mL) with ultrasonic treatment for 2 h. Then, with vigorous stirring, aqueous NaOH solution (0.125 mol/L) was added dropwise into the mixture until the pH value was 10. After stirring for 30 min, the suspension was transferred to a stainless steel autoclave for the hydrothermal process at 110 °C for 24 h. Third, the solid was collected by filtration, repeatedly washed with deionized water and anhydrous ethanol until the pH was 7, and then dried at 80 °C. Finally, the solid was calcined at 500 °C for 4 h in air using a heating rate of 5 °C/min. The sample was denoted as CeO_2-NT.

The preparation of Pd-O/CeO_2-NT was similar to the preparation of CeO_2-NT above. The only difference was that an amount of $PdCl_2$ in aqueous ammonia, along with the suspension, was also added into the autoclave for the hydrothermal process. The other operation processes were the same as those for the preparation of CeO_2-NT. The obtained sample was denoted as Pd-O/CeO_2-NT with a nominal Pd loading of 1.0 wt%.

For comparison with Pd-O/CeO_2-NT, a Pd-O/CeO_2-P catalyst in which CeO_2 was zero-dimensional particles was prepared using a water-in-oil microemulsion as a nanoreactor. The microemusion consisted of cyclohexane (100 mL), Triton X-100 (10.8 mL), $PdCl_2$ in aqueous ammonia (0.25 mmol $PdCl_2$, 10 mL aqueous ammonia), and *n*-hexanol (2.8 mL). $Ce(NO_3)_3$ aqueous solution (3 mL, 5.2 mol/L) was added to the microemulsion and hydrolyzed at 30 °C for 5 h. Then, the solution was centrifuged to separate the precipitate, which was thoroughly washed with ethanol and deionized water, dried at 80 °C overnight, and calcined in the air at 500 °C for 4 h. The sample was denoted as Pd-O/CeO_2-P with a nominal Pd loading of 1.0 wt%.

2.2. Catalyst characterization

Transmission electron microscope (TEM) images and selected area electron diffraction (SAED) were obtained with a PHILIPS TECNOL 20 at an acceleration voltage of 200 kV. The specific surface areas of the samples were calculated by the BET method by N_2 adsorption-desorption with a Micromeritics ASAP 2020 M+C porosity analyzer. X-ray diffraction (XRD) patterns were recorded on a Rigaku D/Max-2500 X-ray diffractometer with Cu K_α (40 kV, 100 mA) radiation and a secondary beam graphite monochromator (SS/DS = 1°, RS 0.15 mm, Counter SC) at the scanning 2θ range of 5°–90°. Raman spectra were measured by a Renishaw inVia Reflex microspectrometer. The Pd content in the catalyst was determined by a Thermo Scientific iCAP 7400 ICP-OES.

Temperature-programmed reduction by hydrogen (H_2-TPR) was carried out on a Micromeritics Auto Chem II-2920 apparatus. All samples (0.1 g) were pretreated in the flow of Ar (50 mL/min) at room temperature for 5 min. Then the flowing gas was switched to 10% H_2/Ar mixture (50 mL/min) and the sample was heated to 1000 °C at a ramping rate of 10 °C/min. The H_2 consumption was monitored by a thermal conductivity detector (TCD).

2.3. Catalyst evaluation

Oxidative carbonylation of phenol was performed in a 50-mL Teflon-lined stainless steel autoclave with a magnetic

stirrer. In a typical experiment, the catalyst and co-catalyst ($Cu(OAc)_2$, tetrabutylammonium bromide, and hydroguinone) along with phenol and the solvent (dichloromethane) and 4A molecular sieve were introduced into the autoclave. Then, the autoclave was pressurized with a mixture of CO and O_2. At the end of the reaction, the autoclave was cooled to room temperature and vented. The catalyst and 4A molecular sieve were removed by filtration.

The product mixture was identified qualitatively using a Thermo Fisher TRACE DSQ GC-MS with a BPX5 (30 m × 0.25 mm × 0.25 μm) capillary column. The injection port temperature was 250 °C. The column temperature was programed and the initial column temperature was fixed at 40 °C for 3 min and then increased to 250 °C at a rate of 10 °C/min. The final temperature was maintained for 5 min. The carrier gas was He at a constant flow of 1 mL/min. A mass spectrometer was used in the electron impact (EI) mode at 200 °C.

A Knauer K2600 HPLC was used to analyze the reaction liquid quantitatively. The analytical conditions were as follows: a Venusil XBP C18 (4.6 mm × 150 mm, 5 μm) chromatographic column was used at a flow rate of 0.6 mL/min. CH_3OH/H_2O (65/35, *V*/*V*) was used as the mobile phase and the detection wavelength was 254 nm. The column temperature was kept at 30 °C and the injection was 20 μL. Quantitative analysis of diphenyl carbonate and phenol was carried out using the external standard method.

3. Results and discussion

3.1. Catalyst characterization

TEM images of CeO_2 and the supported Pd catalysts were recorded and shown in Fig. 1. Figures 1(a) and 1(b) are images of CeO_2-NT, which displayed the outer diameter of 25 nm and lengths of more than 300 nm with open ends. The tube wall was composed of CeO_2 particles with the size of 4–9 nm. The selected area electron diffraction (SAED) pattern of CeO_2-NT is also shown in Fig. 1(b). Its ring diffraction indicated the polycrystalline structure of CeO_2-NT. Moreover, the rings were not smooth with clear spots, which was due to the small amount of CeO_2 crystals in the small selected area diffraction electron beam. The TEM image of Pd-O/CeO_2-NT is shown in Fig. 1(c). The tubular structure of CeO_2 was retained. However, it was difficult to distinguish Pd particles from the CeO_2 support. This may be attributed to the strong interaction between Pd and CeO_2, which inhibited the growth of the Pd particles. On the other hand, the high electron density of CeO_2 also adversely affected finding Pd particles in the TEM image [32]. Boronin et al. [33] indicated that most of the Pd particles on a CeO_2 support could not be observed, even when HR-TEM was utilized. Figure 1(d) is the TEM image of Pd-O/CeO_2-P prepared by the microemulsion method. The sizes of the zero-dimensional CeO_2 particles were 7 to 15 nm. Similarly, Pd particles could not be observed.

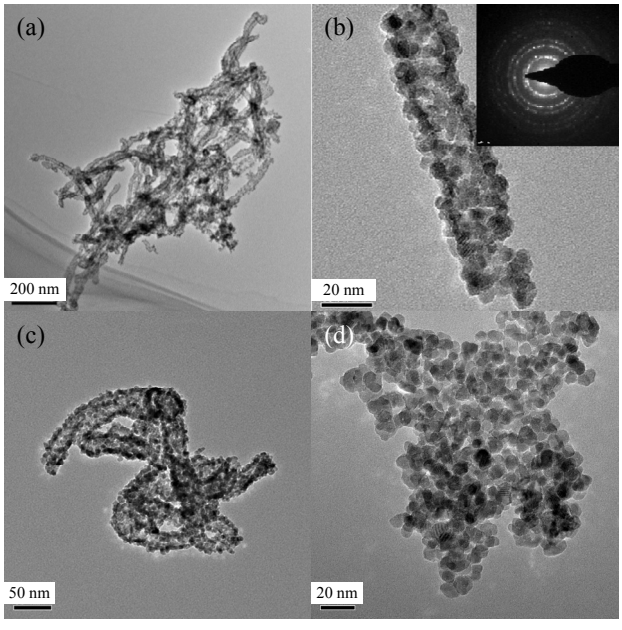

Fig. 1. TEM images of CeO_2 and supported Pd catalyst. (a, b) CeO_2-NT; (c) Pd-O/CeO_2-NT; (d) Pd-O/CeO_2-P; Inset of (b): SAED pattern of CeO_2-NT.

The XRD patterns of Pd-O/CeO_2-NT and Pd-O/CeO_2-P are shown in Fig. 2. There was no significant difference between the two patterns. The peaks at 2θ = 28.48°, 33.12°, 47.59°, 56.46°, 59.07°, 69.44°, 76.75°, and 79.16° were attributed, respectively, to the diffraction of the (111), (200), (220), (311), (222), (400), (331), and (420) planes of CeO_2 with the cubic structure (JCPDS 65-5923). Diffraction peaks for Pd compounds were not found in XRD patterns, possibly because of the high dispersion of the Pd particles of low weight content on the CeO_2 support [34].

The lattice parameter of CeO_2 in Pd-O/CeO_2-NT (0.5402 nm) was smaller than that in Pd-O/CeO_2-P (0.5406 nm), which is shown in Table 1. This indicated that more Ce^{4+} ions were substituted by Pd^{2+} or Pd^{4+} ions in Pd-O/CeO_2-NT. Because the radius of the Pd^{2+} ion (0.84 Å) or Pd^{4+} ion (0.62 Å) is smaller than that of Ce^{4+} (0.99 Å), Pd-O/CeO_2-NT has a small lattice parameter.

The surface area and porosity of the Pd-O/CeO_2-NT and Pd-O/CeO_2-P catalysts were investigated by N_2 adsorption-desorption at −196 °C. As displayed in Fig. 3, both samples exhibit type IV adsorption isotherms with hysteresis loops, which are due to capillary condensation in mesoporous pores [35].

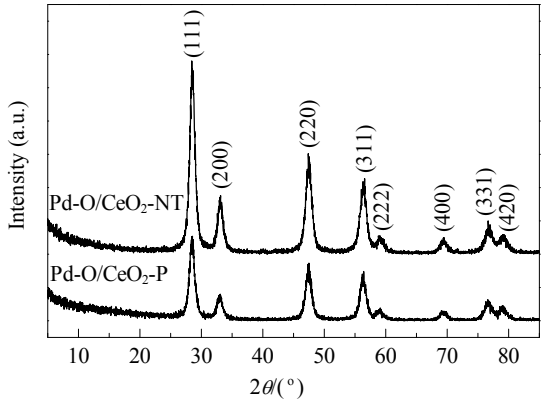

Fig. 2. XRD patterns of the Pd-O/CeO_2 catalysts.

Table 1
Textural properties and catalytic performance of Pd-O/CeO_2 for oxidative carbonylation of phenol.

Catalyst	A_{BET} (m^2/g)	Pore size (nm)	Pore volume (cm^3/g)	Lattice parameter (nm)	Phenol conversion (%)	DPC selectivity (%)
Pd-O/CeO_2-NT	108.8	14.7	0.4	0.5402	53.9	70.9
Pd-O/CeO_2-P	93.8	5.9	0.2	0.5406	25.0	30.5

Reaction conditions: 100 °C, 8 h, O_2 0.6 MPa, CO 6.6 MPa, phenol 25.5 mmol, 20 mL CH_2Cl_2, 0.4 g catalyst (Pd 0.04 mmol), 4.0 g 4A molecular sieve, Pd/$Cu(OAc)_2$/TBAB/H_2BQ = 1/5/40/40 in molar ratio.

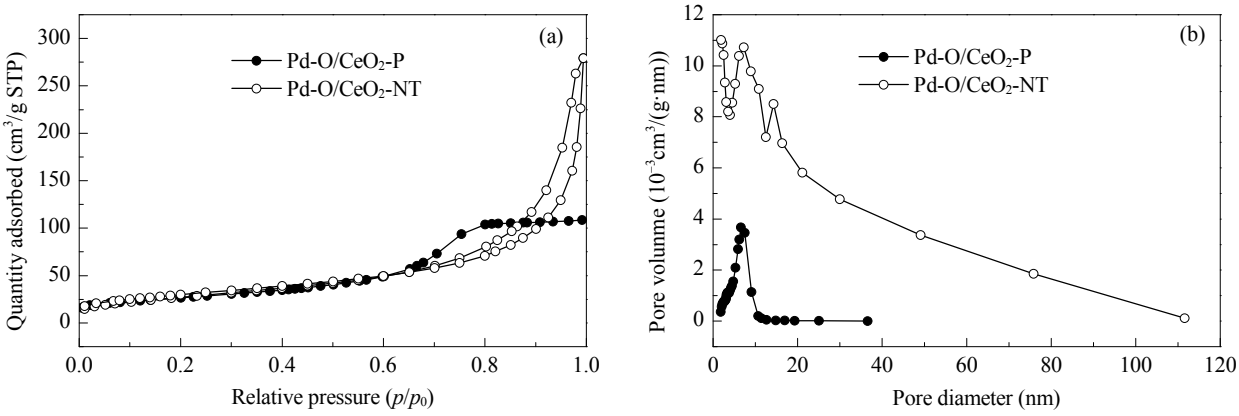

Fig. 3. N_2 adsorption-desorption isotherms (a) and pore size distribution (b) of the Pd-O/CeO_2 catalyst.

The hysteresis loops of Pd-O/CeO_2-NT and Pd-O/CeO_2-P were H3 type and H2 type, respectively, which suggested different pore structures. Figure 3 also shows that the pore size distribution of Pd-O/CeO_2-NT was in a relatively large scale and the pores of Pd-O/CeO_2-P were small and uniform in the mesoporous range. Moreover, the specific surface area of Pd-O/CeO_2-NT (108.8 m^2/g) was larger than that of Pd-O/CeO_2-P (93.8 m^2/g), which was due to its unique tubular structure and small CeO_2 particles.

3.2. Catalytic activity

The two CeO_2 supported Pd catalysts were evaluated for their activity in the oxidative carbonylation of phenol to DPC. The results are shown in Table 1. The Pd-O/CeO_2-NT catalyst was superior to Pd-O/CeO_2-P in both phenol conversion and DPC selectivity.

To explain the difference between the catalytic performance of the two catalysts, H_2-TPR of the catalysts and CeO_2 was carried out. The results are shown in Fig. 4 and Table 2. Two reduction peaks were observed at 478 and 810 °C over CeO_2-P. For CeO_2, the low temperature peak at 400–600 °C was due to the reduction of surface oxygen species attached to surface Ce^{4+} ions in an octahedral coordination and the high temperature peak over 700 °C was due to the reduction of oxygen anion bonded to two Ce^{4+} ions in the bulk phase [36,37]. In the TPR curve of CeO_2-NT, there was an extra strong peak at 307 °C in addition to the surface oxygen peak at 430 °C and the bulk phase oxygen peak at 815 °C. The H_2 consumption corresponding to the reduction peaks (Table 2) suggested that the bulk oxygen contents in CeO_2-P and CeO_2-NT were almost the same. However, the surface oxygen content in CeO_2-NT was much lower than that in CeO_2-P. However, if the H_2 consumption of the reduction peak at 307 °C was taken into account, the surface oxygen content of CeO_2-NT (503.1 μmol/g) approximately equals to that of CeO_2-P (515.4 μmol/g). Thus, the peak at 307 °C was ascribed to a kind of surface oxygen species that can be reduced more easily. The new surface oxygen species was denoted as surface O-II. Its generation is due to the special tubular structure of CeO_2-NT. Furthermore, this implies that the surface oxygen on CeO_2-NT can participate in the catalytic reaction more readily than CeO_2-P. Zhou et al. [30] prepared a kind of highly reducible CeO_2 nanotubes and found that its surface oxygen reduction started at 200 °C. Shan et al. [38] also found surface oxygen species that could be reduced at 180 °C in their 3D CeO_2. They attributed this to the increase of surface oxygen vacancies on CeO_2, which can activate molecular oxygen easily, which then resulted in more adsorbed oxygen species that can be easily reduced. Rao [39] believed that the reduction temperature of the CeO_2 surface oxygen was related to the coordination number of O^{2-}. The less coordinated oxygen species are reduced at a lower temperature than those with a higher coordination.

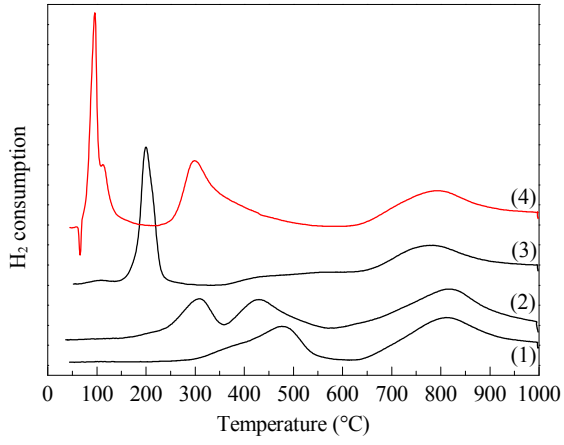

Fig. 4. TPR profiles of CeO_2 and Pd-O/CeO_2. (1) CeO_2-P; (2) CeO_2-NT; (3) Pd-O/CeO_2-P; (4) Pd-O/CeO_2-NT.

Table 2
H_2-TPR results of CeO_2 and Pd-O/CeO_2.

Sample	Peak temperature (°C)				H_2 uptake (μmol/g)			
	Mixed O*	Surface O-II	Surface O	Bulk O	Mixed O	Surface O-II	Surface O	Bulk O
CeO_2-P	—	—	478	810	—	—	515.4	663.7
CeO_2-NT	—	307	430	815	—	226.8	276.3	663.5
Pd-O/CeO_2-P	200	—	432	778	520.2	—	75.8	448.9
Pd-O/CeO_2-NT	—	96	299	785	—	603.2	747.5	570.9

* Sum of redution of PdO and surface O.

The TPR profiles of the CeO_2 supported Pd catalyst changed significantly compared with those of CeO_2. The surface oxygen peak became very weak with a H_2 consumption of 75.8 μmol/g in the TPR curve of Pd-O/CeO_2-P. Moreover, there were two other reduction peaks at 200 and 778 °C. The latter was ascribed to the reduction of the bulk oxygen of CeO_2. The former was considered as the sum of the reduction of PdO and surface oxygen [40]. Since the reduction temperature of PdO is 50 °C [41], the interaction between PdO and CeO_2-P hindered the reduction of PdO [40]. This would also account for the decrease of the reduction temperature of the CeO_2 surface oxygen species from 478 to 200 °C.

In the Pd-O/CeO_2-NT the bulk oxygen reduction temperature was 785 °C, and the surface oxygen reduction temperature decreased to 299 °C. There was another strong reduction peak at 96 °C. Furthermore, a reverse peak at 65 °C indicated that the sample released H_2. This can be explained by the fact that metal Pd can adsorb H_2 to form a hydride (PdH_x) at room temperature under 0.013 atm H_2 pressure [42]. PdH_x decomposed to release H_2 at an elevated temperature. This also revealed that the Pd species on the Pd-O/CeO_2-NT surface could be reduced at an even lower temperature. Cargnello et al. [43] found that PdO/CeO_2 prepared by impregnation could be reduced to Pd/CeO_2 at room temperature. This was also the case of TiO_2 supported Pd catalyst [40]. This was attributed to the highly dispersed Pd species on the support. This also suggested that the peak at 96 °C corresponded to the reduction of surface O–II only and did not include the reduction of PdO. It can be suggested that the decrease of the surface oxygen reduction temperature in Pd-O/CeO_2-NT was the result of hydrogen spillover [41]. From the data in Table 2, it can be found that the hydrogen consumption by the surface oxygen species on Pd-O/CeO_2-NT increased (1350.7 μmol/g) compared with those of CeO_2-NT (503.1 μmol/g) and Pd-O/CeO_2-P (596.0 μmol/g). This can be assigned to the increase of oxygen vacancies on the surface of Pd-O/CeO_2-NT. Figure 5 shows the Raman spectra of the catalysts with a 325-nm excitation laser line. It can be seen that all the catalysts have two distinct bands at 449 and 581 cm^{-1}. The former is ascribed to the Raman active F_{2g} mode vibration of CeO_2, and the latter is attributed to oxygen vacancies [44]. The peak areas of the two bands were calculated and the results shown in Fig. 5, which are denoted as A449 and A581, respectively. The ratio of A581/A449 revealed the concentration of oxygen vacancies in the catalyst. It can be seen that the A581/A449 value for Pd-O/CeO_2-NT (0.58) was higher than that for Pd-O/CeO_2-P (0.43), reflecting that there was a higher concentration of oxygen vacancies in the Pd-O/CeO_2-NT catalyst. According to the XRD result, there were more Ce^{4+} substituted by Pd^{2+}/Pd^{4+} in Pd-O/CeO_2-NT, which led to more oxygen vacancies [45]. O_2 can be adsorbed on oxygen vacancies to generate the oxygen species that can be reduced easily [38]. Furthermore, the H_2 consumption may also be generated by the spillover of hydrogen atoms, which originated from H_2 dissociative adsorption on the highly dispersed metallic Pd onto the surface of CeO_2.

According to the above TPR results, the Pd-O/CeO_2-NT catalyst showed a high phenol conversion because of increased surface oxygen species. Meanwhile, there was a strong interaction between the highly dispersed Pd and CeO_2. This favored electron transfer from Pd(0) to Ce(IV); therefore the active sites can be regenerated to Pd(II), which promoted the synthesis of DPC and increased its selectivity.

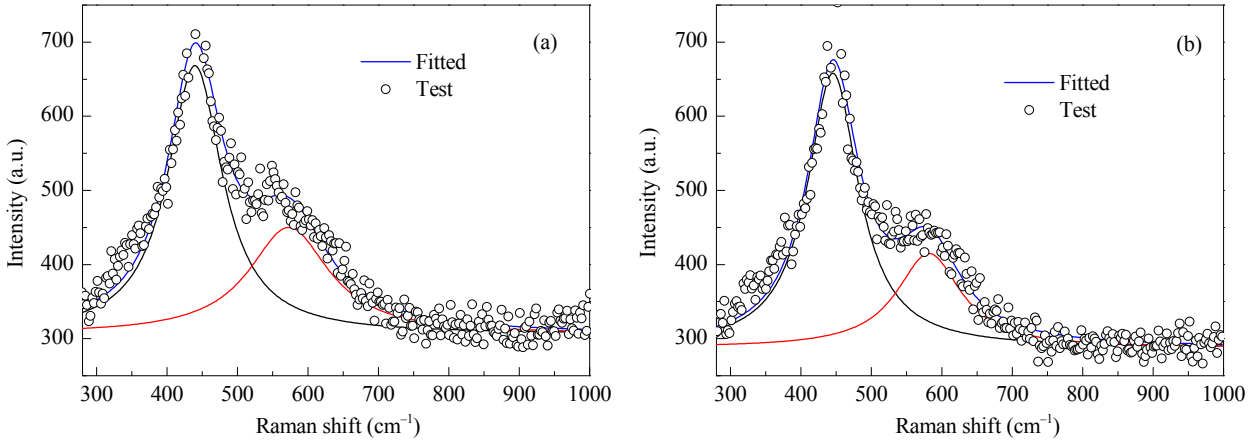

Fig. 5. Raman spectra of Pd-O/CeO_2-NT (a) and Pd-O/CeO_2-P (b).

3.3. Oxidative carbonylation of phenol catalyzed by Pd-O/CeO_2-NT

3.3.1. Effect of reaction time

The influence of reaction time on the oxidative carbonylation of phenol over the Pd-O/CeO_2-NT catalyst was studied. The results are shown in Fig. 6. Phenol conversion increased quickly from 23.3% to 58.2% as the reaction time was extended from 5 to 8 h. However, the DPC selectivity changed in a different way from the phenol conversion. The DPC selectivity was 96.3% when the reaction time was 5 h. With the prolonging of time, the DPC selectivity gradually decreased. In particular, there was an obvious decrease from 93.6% to 86.8% when the time was changed from 7 to 8 h. During the reaction, phenol can be oxidized by O_2 to benzoquinone and dimeric and trimeric compounds and polymers, which was proved by the brown reaction solution. The polymers can accumulate on the catalyst surface and cover the active sites. Therefore, DPC synthesis was decreased when the reaction time was increased. However, the side reactions were less influenced and phenol conversion still increased. As a result, the DPC selectivity decreased gradually with reaction time. Moreover, DPC can react with H_2O, another product of the oxidative carbonylation reaction, to give the formation of phenol and CO_2. This also decreased the DPC selectivity.

3.3.2. Effect of reaction temperature

The effect of reaction temperature on the oxidative carbonylation of phenol over Pd-O/CeO_2-NT catalyst is shown in Fig. 7. Phenol conversion gradually increased from 17.7% to 60.7% as the reaction temperature increased from 80 to 110 °C. Meanwhile, DPC selectivity increased from 88.1% to 95.3%. With further temperature elevation to 120 °C, the phenol conversion changed little and DPC selectivity decreased to 85.7%. The oxidative carbonylation of phenol is an exothermic reaction. A high temperature would retard the reaction by decreasing the equilibrium constant. However, from the viewpoint of reaction kinetics, a high temperature accelerates the reaction rate. Therefore, there is an optimum reaction temperature for the oxidative carbonylation of phenol. Furthermore, phenol is easily oxidized by O_2 at a high temperature to generate polymer sideproducts, which would cover the active sites of the catalyst and prevent the formation of DPC. Then the DPC selectivity decreased.

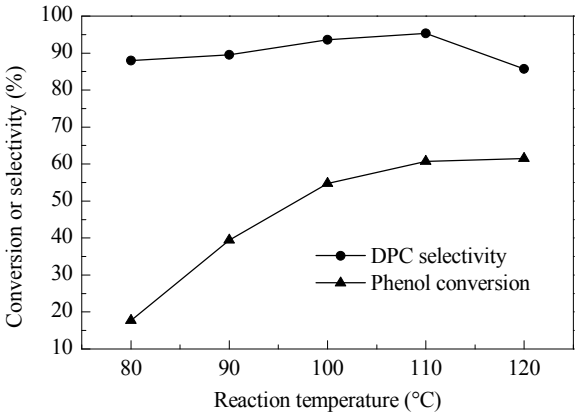

Fig. 7. Effect of reaction temperature on oxidative carbonylation of phenol. Reaction conditions: 7 h, O_2 0.6 MPa, CO 6.6 MPa, phenol 25.5 mmol, 20 mL CH_2Cl_2, 0.4 g catalyst (Pd 0.04 mmol), 4.0 g 4A molecular sieve, Pd/$Cu(OAc)_2$/TBAB/H_2BQ = 1/5/40/40 in molar ratio.

3.3.3. Effect of reaction pressure

Figure 8 shows the effect of reaction pressure on the oxidative carbonylation of phenol. The partial pressure ratio of CO/O_2 was kept at 11/1 to ensure that the CO concentration was beyond the explosive limit. Phenol conversion increased from 41.3% to 60.7% as the CO pressure changed from 4.4 to 6.6 MPa. After that, it remained unchanged with the further increase of CO pressure. The DPC selectivity decreased from 97.2% to 87.7% when the CO pressure increased from 4.4 to 7.7 MPa. In a volume-reduced reaction with gaseous reactants, such as the oxidative carbonylation of phenol, a higher pressure can accelerate the reaction. CO adsorption on the catalyst is also promoted at a higher pressure with the result of increasing phenol conversion. When the CO adsorption reaches saturation on the catalyst surface as the pressure increases, the

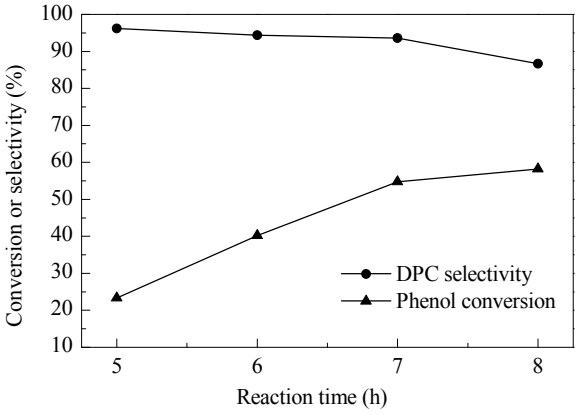

Fig. 6. Effect of reaction time on oxidative carbonylation of phenol. Reaction conditions: 100 °C, O_2 0.6 MPa, CO 6.6 MPa, phenol 25.5 mmol, 20 mL CH_2Cl_2, 0.4 g catalyst (Pd 0.04 mmol), 4.0 g 4A molecular sieve, Pd/$Cu(OAc)_2$/TBAB/H_2BQ = 1/5/40/40 in molar ratio.

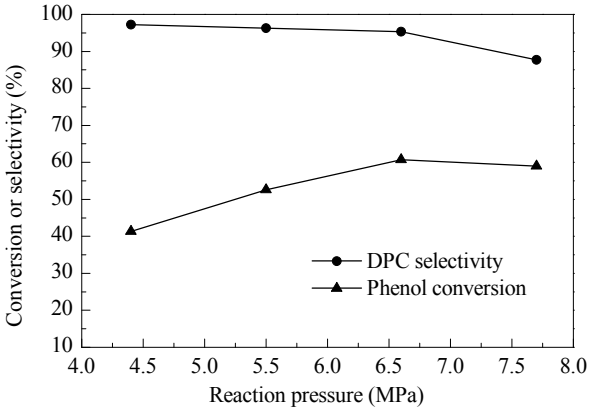

Fig. 8. Effect of reaction pressure on oxidative carbonylation of phenol. Reaction conditions: 110 °C, 7 h, phenol 25.5 mmol, 20 mL CH_2Cl_2, 0.4 g catalyst (Pd 0.04 mmol), 4.0 g 4A molecular sieve, Pd/$Cu(OAc)_2$/TBAB/H_2BQ = 1/5/40/40 in molar ratio.

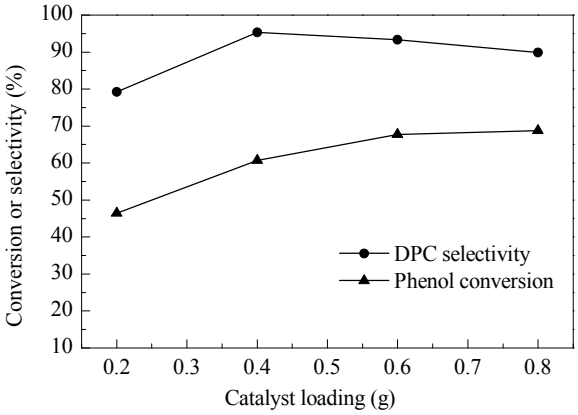

Fig. 9. Effect of catalyst loading on oxidative carbonylation of phenol. Reaction conditions: 110 °C, 7 h, O_2 0.6 MPa, CO 6.6 MPa, phenol 25.5 mmol, 20 mL CH_2Cl_2, 4.0 g 4A molecular sieve, $Pd/Cu(OAc)_2/TBAB/H_2BQ$ = 1/5/40/40 in molar ratio.

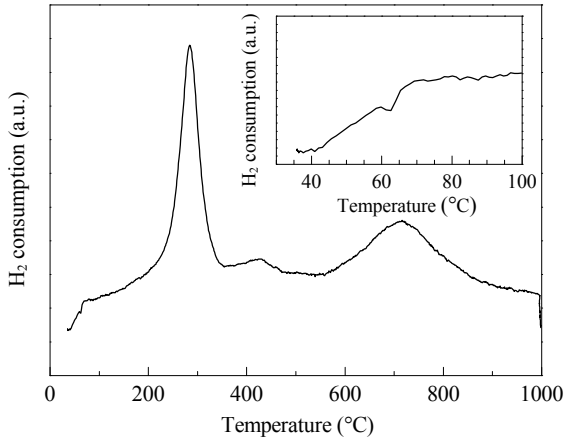

Fig. 11. TPR profile of once used Pd-O/CeO_2-NT.

phenol conversion then remains constant. In addition, the side reactions of phenol oxidation can also be accelerated with increasing pressure. The side reactions occur much more easily than DPC synthesis. Thus the DPC selectivity decreased with increasing pressure.

3.3.4. Effect of catalyst loading

The effect of Pd-O/CeO_2-NT catalyst loading on the oxidative carbonylation of phenol was investigated. The results are shown in Fig. 9. Phenol conversion increasesd from 46.4% to 68.8% with increasing catalyst loading due to the increase of active sites. The DPC selectivity, however, increased at first and then decreased gradually. This indicated that some side reactions were accelerated also. An overall consideration of phenol conversion and DPC selectivity showed that the optimal catalyst loading was 0.6 g (Pd/phenol = 1/425, molar ratio) under the given conditions. The optimized results were as follows. Phenol conversion was 67.7% with 93.3% DPC selectivity, and the turnover frequency (TOF) was 38.3 mol-DPC/(mol-Pd·h).

3.3.5. Catalyst reusability

After the reaction, the Pd-O/CeO_2-NT catalyst was washed with ethanol throughly, dried at 80 °C, and calcined at 500 °C for 1 h to eliminate residual organic compounds. Then it was re-evaluated for the oxidative carbonylation of phenol to DPC. The results showed that only 29.3% phenol was converted with 62.3% DPC selectivity. That is, Pd-O/CeO_2-NT has partly lost its catalytic activity. The TEM image of the once-used Pd-O/CeO_2-NT was recorded to reveal its change. This is shown in Fig. 10. Compared with Fig. 1(c), it can be concluded that most of the CeO_2 nanotubes had collapsed into small particles during the reaction. The TPR curve of the once-used Pd-O/CeO_2-NT is shown in Fig. 11. The peak corresponding to the reduction of surface O-II at 96 °C in the TPR curve of the fresh Pd-O/CeO_2-NT has disappeared, while the peaks assigned to the decomposition of PdH_x, surface oxygen, and bulk oxygen still existed. This is evidence that surface O-II was generated by the special structure of Pd-O/CeO_2-NT. Due to the destruction of the nanotube during the reaction, Pd-O/CeO_2-NT has lost its activity. In addition, ICP analysis was conducted to show Pd leaching during the reaction. The results showed there were 0.56% and 0.36% Pd content in the fresh and once-used Pd-O/CeO_2-NT, respectively. Therefore, this was also a cause of the deactivation.

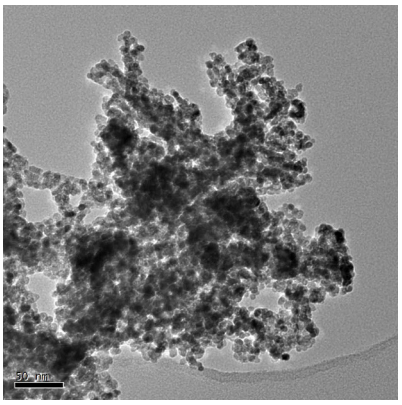

Fig. 10. TEM image of once used Pd-O/CeO_2-NT.

4. Conclusions

CeO_2 nanotubes (CeO_2-NT) were prepared by a liquid phase deposition-hydrothermal method using CNTs as the template. The CeO_2-NT has outer diameters of about 25 nm and lengths of more than 300 nm. A Pd-O/CeO_2-NT catalyst was prepared using the CeO_2-NT as support, which has surface oxygen species that can be reduced at a lower temperature. This led to a high activity in the catalytic reaction. Pd-O/CeO_2-NT was used as the catalyst for the oxidative carbonylation of phenol and it gave better activity and DPC selectivity than Pd-O/CeO_2-P. When the CO pressure was 6.6 MPa and catalyst loading was Pd/phenol = 1/425 (molar ratio), the phenol conversion was 67.7% with 93.3% DPC selectivity at 110 °C after 7 h. After the reaction, the tubular structure of Pd-O/CeO_2-NT was destroyed and the surface oxygen species that was reduced at a lower temperature disappeared. Moreover, Pd leaching also occurred during the reaction. All these resulted in a decrease of the catalytic performance of Pd-O/CeO_2-NT.

Graphical Abstract

Chin. J. Catal., 2015, 36: 1142–1154 doi: 10.1016/S1872-2067(14)60312-0

Oxidative carbonylation of phenol with a Pd-O/CeO_2-nanotube catalyst

Ye Yuan, Zhimiao Wang, Hualiang An, Wei Xue *, Yanji Wang *
Hebei University of Technology

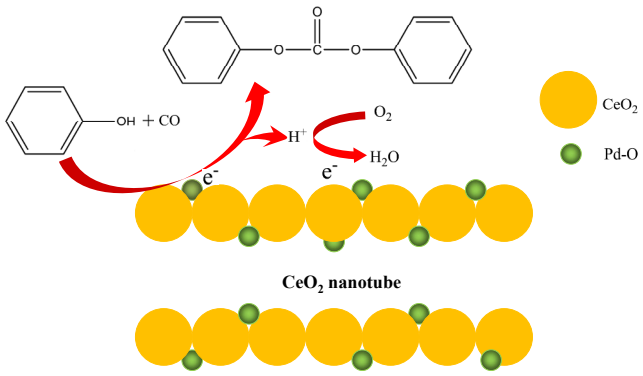

CeO_2 nanotubes (CeO_2-NT) as the support for a Pd catalyst, Pd-O/CeO_2-NT, gave high phenol conversion with high dipenyl carbonate selectivity in the oxidative carbonylation of phenol.

References

[1] Wang Y J, Zhao X Q. Green Catalytic Chemical Process and Technology. Beijing: Chem Ind Press, 2002. 160
[2] Gong J L, Ma X B, Wang S P. *Appl Catal A*, 2007, 316: 1
[3] Xue W, Teng Z, Wang Z M, Yuan Y, Zhang D S, Wang Y J. CN Patent 103611532 A. 2013
[4] Zhou W Q, Zhao X Q, Wang Y J, Zhang J Y. *Appl Catal A*, 2004, 260: 19
[5] Zhou X, Ge X, Tang R Z, Chen T, Wang G Y. *Chin J Catal*, 2014, 35: 481
[6] Hallgren J E, Lucas G M, Matthews R O. *J Organomet Chem*, 1981, 204: 135
[7] Vavasori A, Toniolo L. *J Mol Catal A*, 1999, 139: 109
[8] Goyal M, Nagahata R, Sugiyama J, Asai M, Ueda M, Takeuchi K. *Catal Lett*, 1998, 54: 29
[9] Linsen K J L, Libens J, Jacobs P A. *Chem Commun*, 2002: 2728
[10] Xue W, Zhang J C, Wang Y J, Zhao Q, Zhao X Q. *J Mol Catal A*, 2005, 232: 77
[11] Song H Y, Park E D, Lee J S. *J Mol Catal A*, 2000, 154: 243
[12] Ishii H, Takeuchi K, Asai M, Ueda M. *Catal Commun*, 2001, 2: 145
[13] Zhang G X, Wu Y X, Ma P S, Wu G W, Li D H. *Chin J Catal*, 2002, 23: 130
[14] Kim W B, Park E D, Lee C W, Le J S. *J Catal*, 2003, 218: 334
[15] Fan G Z, Huang J, Li Z Q, Li T, Li G X. *J Mol Catal A*, 2007, 267: 34
[16] Lu W, Du Z P, Yuan H, Tian Q F, Wu Y X. *Chin J Chem Eng*, 2013, 21: 8
[17] Yang X J, Han J Y, Du Z P, Yuan H, Jin F, Wu Y X. *Catal Commun*, 2010, 11: 643
[18] Ronchin L, Vavasori A, Amadio E, Cavinato G, Toniolo L. *J Mol Catal A*, 2009, 298: 23
[19] Xue W, Zhang J C, Wang Y J, Zhao X Q, Zhao Q. *Catal Commun*, 2005, 6: 431
[20] Zhang Y L, Xiang S L, Wang G Q, Jiang H, Xiong C R. *Catal Sci Technol*, 2014, 4: 1055
[21] Wu M, Yuan H, Du Z P, Wu Y X. *Appl Chem Ind*, 2008, 37: 990
[22] Wang Z M. [MS Dissertation]. Tianjin: Hebei Univ Technol, 2012
[23] Ta N, Liu J Y, Shen W J. *Chin J Catal*, 2013, 34: 838
[24] Li Y, Shen W J. *Sci Sin Chim*, 2012, 42: 376
[25] Liu L J, Cao Y, Sun W J, Yao Z J, Liu B, Gao F, Dong L. *Catal Today*, 2011, 175: 48
[26] Wu Z L, Li M J, Overbury S H. *J Catal*, 2012, 285: 61
[27] Wang S P, Zhao L F, Wang W, Zhao Y J, Zhang G L, Ma X B, Gong J L. *Nanoscale*, 2013, 5: 5582
[28] Pan C S, Zhang D S, Shi L Y, Fang J H. *Eur J Inorg Chem*, 2008: 2429
[29] Shan W J, Liu C, Guo H J, Yang L H, Wang X N, Feng Z C. *Chin J Catal*, 2011, 32: 1336
[30] Zhou K B, Yang Z Q, Yang S. *Chem Mater*, 2007, 19: 1215
[31] Zhang D S, Fu H X, Shi L Y, Fang J H, Li Q. *J Solid State Chem*, 2007, 180: 654
[32] Cargnello M, Doan-Nguyen V V T, Gordon T R, Diaz R E, Stach E A, Gorte R J, Fornasiero P, Nurray C B. *Science*, 2013, 341: 771
[33] Boronin A I, Slavinskaya E M, Danilova I G, Gulyaev R V, Amosov Y I, Kuznetsov P A, Polukhina I A, Koscheev S V, Zaikovskii V I, Noskov A S. *Catal Today*, 2009, 144: 201
[34] Tang Z R, Yin X, Zhang Y H, Zhang N, Xu Y J. *Chin J Catal*, 2013, 34: 1123
[35] Sing K S W, Everett D H, Haul R A W, Moscou L, Pierotti R A, Rouquérol J, Siemieniewska T. *Pure Appl Chem*, 1985, 57: 603
[36] Yao H C, Yu Yao Y F. *J Catal*, 1984, 86: 254
[37] Li J, Ta N, Li Y, Shen W J. *Chin J Catal*, 2008, 29: 823
[38] Shan W J, Dong X W, Ma N, Yao S Y, Feng Z C. *Catal Lett*, 2009, 131: 350
[39] Rao G R. *Bull Mater Sci*, 1999, 22: 89
[40] Zhu H Q, Qin Z F, Shan W J, Shen W J, Wang J G. *J Catal*, 2004, 225: 267
[41] Luo M F, Hou Z Y, Yuan X X, Zheng X M. *Catal Lett*, 1998, 50: 205
[42] Amorim C, Wang X D, Keane M A. *Chin J Catal*, 2011, 32: 746
[43] Cargnello M, Montini T, Polizzi S, Wieder N L, Gorte R J, Graziani M, Fornasiero P. *Dalton Trans*, 2010, 39: 2122
[44] Meng L, Jia A P, Lu J Q, Luo L F, Huang W X, Luo M F. *J Phys Chem C*, 2011, 115: 19789
[45] Reddy B M, Katta L, Thrimurthulu G. *Chem Mater*, 2010, 22: 467

Page numbers refer to the contents in the print version, which include both the English and Chinese versions of the paper. The online version only has the English version. The pages with the Chinese version are only available in the print version.